Protein Microgels from Amyloid Fibril Networks

Ulyana Shimanovich,[†] Igor Efimov,[†] Thomas O. Mason,[†] Patrick Flagmeier,[†] Alexander K. Buell,[†] Aharon Gedanken,[‡] Sara Linse,[§] Karin S. Åkerfeldt,[⊥] Christopher M. Dobson,[*,†] David A. Weitz,[*,∥] and Tuomas P. J. Knowles[*,†]

[†]Department of Chemistry, University of Cambridge, Lensfield Road, Cambridge CB2 1EW, U.K., [‡]Department of Chemistry, Bar-Ilan University, Ramat-Gan 52900, Israel, [§]Department of Biochemistry and Structural Biology, Lund University, Lund 22100, Sweden, [⊥]Department of Chemistry, Haverford College, Haverford, Pennsylvania 19041, United States, and [∥]Department of Physics and School of Engineering and Applied Science, Harvard University, 29 Oxford Street, Cambridge, Massachusetts 02138, United States

ABSTRACT Nanofibrillar forms of proteins were initially recognized in the context of pathology, but more recently have been discovered in a range of functional roles in nature, including as active catalytic scaffolds and bacterial coatings. Here we show that protein nanofibrils can be used to form the basis of monodisperse microgels and gel shells composed of naturally occurring proteins. We explore the potential of these protein microgels to act as drug carrier agents, and demonstrate the controlled release of four different encapsulated drug-like small molecules, as well as the component proteins themselves. Furthermore, we show that protein nanofibril self-assembly can continue after the initial formation of the microgel particles, and that this process results in active materials with network densities that can be modulated *in situ*. We demonstrate that these materials are nontoxic to human cells and that they can be used to enhance the efficacy of antibiotics relative to delivery in homogeneous solution. Because of the biocompatibility and biodegradability of natural proteins used in the fabrication of the microgels, as well as their ability to control the release of small molecules and biopolymers, protein nanofibril microgels represent a promising class of functional artificial multiscale materials generated from natural building blocks.

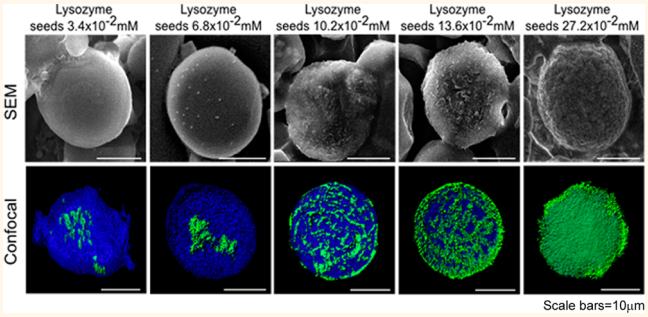

KEYWORDS: microfluidics · protein nanofibrils · microgels · lysozyme · drug release

Amyloid fibrils are a common form of protein nanostructure resulting from the aggregation of soluble proteins into β-sheet rich supramolecular polymers, which possess remarkable physical properties, including a high Young's modulus and tensile strength[1−3] and the ability to self-assemble under mild conditions in aqueous solution.[4,5,7−9] Such structures were initially identified in nature as pathological protein deposits, yet recently have emerged as key functional components in biological materials found in organisms ranging from bacteria to humans.[3,8,10−13] Moreover, artificial variants of these nanoscale materials[3,4,14−17] are finding increasing use as cell culture scaffolds[19] and drug delivery vehicles.[20,21] However, the applications of the general nanofibrillar amyloid scaffold[1,18,29] have been limited by the challenges in enabling the overall micron scale morphology to progress beyond spatially uniform gels. By combining the inherent nanoscale self-assembly process with micron scale structuring, afforded by droplet microfluidics, we establish a class of physical microgels based on nanofibril-forming proteins that are easy to synthesize, biodegradable and nontoxic and that show advantageous characteristics as vehicles for the encapsulation and release of small molecules.[25,26]

Microgels[5,27] combine characteristics from two key classes of soft matter, colloids and polymers, and consist of micron scale particles composed of cross-linked polymer networks that behave as a gel.[27,29] Their ability to respond to environmental stimuli has led to significant efforts to exploit microgels as functional materials. In addition to applications for purposes such as the synthesis of nanoparticles,[29,30] microgels have been found to be highly suitable as agents for drug delivery, as they can be loaded with therapeutic agents[31,32] and designed to

* Address correspondence to cmd44@cam.ac.uk, weitz@seas.harvard.edu, tpjk2@cam.ac.uk.

Received for review August 29, 2014 and accepted December 3, 2014.

Published online 10.1021/nn504869d

transport such agents across biochemical barriers, so as to release them in specifically targeted tissues. Significant progress has been made to template the gelation of proteins using polymeric supporting systems or chemical cross-linkers.[17] A particularly exciting recent development is that of supramolecular microgels which allow a range of macromolecules to be exploited as building blocks.[22−24] In the present work, we demonstrate a different strategy for the synthesis of supramolecular microgels solely from naturally occurring proteins, which is driven by their generic ability to self-assemble into nanoscale filaments under suitable conditions.[33] This approach results in protein microgels where the stabilization of the gel is driven through intrinsic interactions between protein molecules and no extrinsic cross-linking agents are required.

RESULTS AND DISCUSSION

The nanofibril microgel particles were synthesized using a water-in-oil strategy by forming microdroplets of a concentrated aqueous solution of the precursor polypeptide molecule,[34−36] here the abundant natural protein lysozyme, in an immiscible oil phase as a microemulsion created in a microfluidic droplet maker (see Methods). The conversion of the soluble protein into a nanofibril gel[32] was initiated through incubation of the microemulsion at 65 °C as shown in Figure 1a. We here also found that this general fabrication approach (Figure 1a) can be expanded to generate hollow gel shells (Figure 1b, d and f) in addition to dense microgels (Figure 1c and e). To achieve this objective, we inverted the aqueous and oil phases, while otherwise keeping the fabrication protocol identical (Figure 1b). The resulting gel particles were visualized using Nile Red staining[37] of the proteinaceous content followed by examination using confocal fluorescence microscopy (Figure 1c and d). A striking difference in the spatial localization of the fluorescence signal was observed between the microgel particles produced from oil-in-water microdroplets compared to the water-in-oil strategy. Whereas the fluorescence is emitted throughout the volume of the particles in the latter case (Figure 1c), only a fluorescent outer shell is observed in the former case (Figure 1d). This observation, which was confirmed by a complete reconstruction of the particles using z-stacked images (Figure 1c and d), suggests that in the latter case the proteins localize at the oil/water interface when the droplets are synthesized as an oil-in-water emulsion and subsequently form a hollow gel shell, whereas in the former case dense microgel spheres are produced. The localization of the lysozyme fibrils within the microgel particles was visualized using cryo-scanning electron microscopy (Cryo-SEM, see Methods) and shown in Figure 1e and f. The nanofibrillar protein component was detected in the interior of the water-in-oil microgel particles (Figure 1e) and as an outer shell for the oil-in-water microgels (Figure 1f).

Control over the size of the gel particles was achieved by regulating the channel width of the microfluidic droplet maker and the relative flow rates of the oil and aqueous phases (see Methods). In this manner, we tuned systematically the diameter of the gel particles over 2 orders of magnitude, from larger than 60 μm down to 2 μm, Figure 2a and b. The ζ-potential measured for these structures was in all cases positive, as expected for particles formed from a positively charged protein.[38,39]

We generated a range of different morphologies of microgel particles by varying the ratio of free soluble

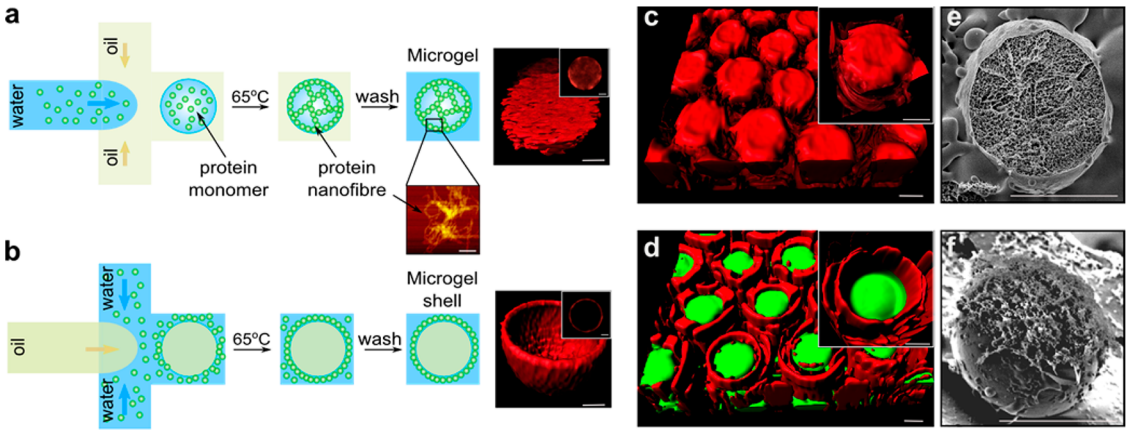

Figure 1. Schematic representation of protein microgel synthesis: (a) Water-in-oil microgels. An atomic force microscopy image of the lysozyme protein nanofibrils is shown at the bottom of the scheme. Scale bar = 400 nm. (b) Oil-in-water microgel shells. The corresponding 3D confocal images of microgel and microgel shell particles stained with Nile Red are shown on the right-hand side of each scheme. (c) 3D reconstructions of the confocal images for lysozyme water-in-oil and (d) oil-in-water capsules stained with Nile Red. The enlarged images of a single microgel and a microgel shell capsule are shown as an insert in the right corner of each image, scale bar = 5 μm. Red emission (excitation at 594 nm/emission at 617 nm) is observed for the aqueous protein component while green emission (excitation at 488 nm/emission 519 nm) is detected for the oil environment. Scale bars = 5 μm. (e) Cryo-scanning electron microscopy images of lysozyme water-in-oil and (f) oil-in-water microgel and microgel shell. Scale bars = 20 μm.

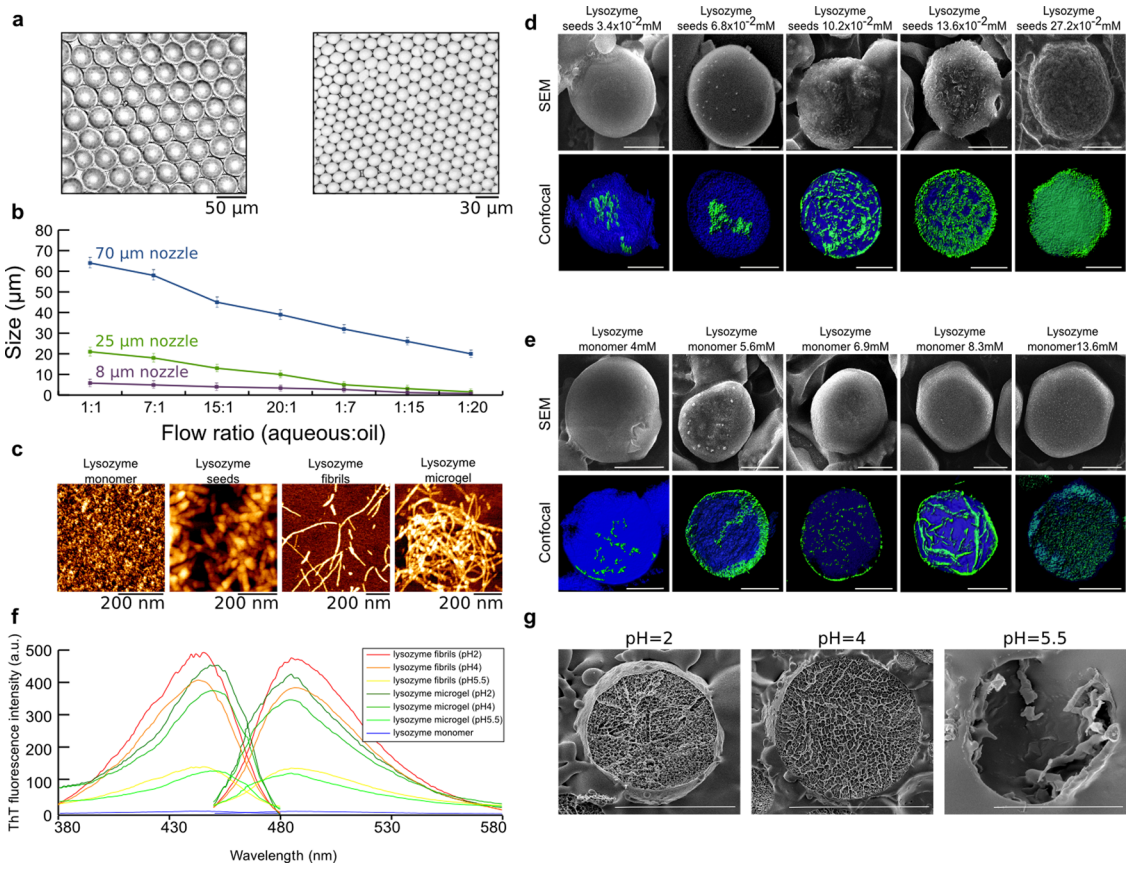

Figure 2. (a) Images from bright field light microscopy of lysozyme microgels of different sizes (from left to right: 49 and 23 μm). (b) Graph showing the change of lysozyme capsule diameter as a function of change in microfluidic channel width and in the aqueous solution: oil ratio. (c) Atomic force microscopy images of lysozyme monomers, seeds, fibrils and microgel. (d) SEM images (top) of lysozyme capsules synthesized with an initial seed concentration of 3.4×10^{-2} mM and a concentration of soluble protein of 4.08 mM, from left to right: seed concentration increased from 3.4×10^{-2} to 27.2×10^{-2} mM. 3D reconstructions of confocal microscopy images (bottom) of the ThT-stained lysozyme capsule synthesized with an initial seed concentration of 3.4×10^{-2} mM and a concentration of soluble lysozyme of 4.08 mM, from left to right: with seeds concentration increased from 3.4×10^{-2} to 27.2×10^{-2} mM. The concentrations are indicated on the top of each image. (e) SEM and confocal images of the ThT stained capsule with increasing lysozyme concentration from 4.08 to 13.6 mM. The blue emission (excitation 350 nm/emission 438 nm) is detected for lysosome protein monomers, green fluorescent emission (excitation 450 nm/emission 482 nm) detected for lysozyme nanofibrils. Scale bars = 10 μm. (f) ThT fluorescence intensity change upon binding to nanofibrillar content of lysozyme protein formed at pH 2,4 and 5.5 and nanofibrillar content of microgel particles formed at pH 2, 4, and 5.5. (g) Cryo-SEM images of microgel particles formed at pH 2, 4 and 5.5.

lysozyme and preformed seed fibrils[40,41] (Figure 2c) introduced into the reaction mixture prior to emulsification. Scanning electron microscopy (SEM: Figure 2d and e) analysis revealed that the surfaces of the particles become rougher, on average, with increasing seed concentration (see seed preparation under Methods). An increase in the initial concentration of monomeric lysozyme, by contrast, has only a small effect on the gel morphology (Figure 2e).

We next imaged the internal structure of the particles with confocal fluorescence microscopy (see Methods section for details), making use of the enhanced and red-shifted fluorescence of ThT consequent upon binding to lysozyme nanofibrils.[42] Figure 2d demonstrates that the fluorescence signal stemming from nanofibril-bound ThT increases systematically with increasing seed concentration. Even in the case of the highest seed concentrations, the added mass concentration due to the seeds amounts to less than 7% of the total protein concentration in the particles, the gelation is therefore driven entirely by the growth of these seed structures rather than by cross-linking of the seeds themselves. Moreover, the images of the particles formed with the highest concentration of seeds (Figure 2d) indicate that the soluble protein has almost quantitatively been transformed into fibrils. In addition, the confocal analysis of the internal microgel structure (Figure 2d) reveals that an increase in seed concentration leads to an increased concentration of protein nanofibrils in the final microgels. An increase in the concentration of soluble protein (Figure 2e), by contrast, does not lead to a systematic increase in fibril content. These results show, therefore, that the internal structure and morphology of the microgels can be controlled by varying the concentrations of soluble lysozyme and seed fibrils in the aqueous phase used

to form the droplets as well as by the incubation time at elevated temperature (65 °C). Interestingly, we observed a decrease in the density of protein nanofibrillar content with an increase in pH of the precursor solution (Figure 2f and g). Thus, microgel particles formed at lower pH (pH 4 and below) showed an increase in the fluorescence intensity of the amyloid-binding ThT dye (Figure 2f) and of the fibrillar density of the particle cores (Figure 2g), while microgel particles formed at pH 5.5 and higher demonstrated low protein nanofibrillar density in the particle cores. The transformation of monomeric lysozyme into nanofibrillar structures in bulk and in microgels was reconfirmed by Fourier transform infrared spectroscopy (FTIR) analysis (see Methods and Supporting Information Figure S1a and b). Moreover, the kinetics of lysozyme gelation in bulk as well as in microdroplets was studied by CD and fluorescence spectroscopy (see Methods and Figure S2). These experiments showed almost no difference in β-sheet content between fibrillar lysozyme in bulk and in microgels formed from a microemulsion.

The component protein molecules were found to be released progressively from the protein microgel particles when they were transferred from their growth environment at pH 2.0 to deionized water. Studies of the release of the protein molecules from the gel particles were conducted by separating the microgels from the solution by centrifugation (see Methods) and measuring the increase in the UV absorption in the soluble phase resulting from the increase in the concentration of soluble protein. The data in Figure 3d reveal that the kinetic profile displays two stages: a fast process taking place over a time scale of less than an hour, which releases 30−50% of the protein content, and a slow phase, which occurs over days to weeks, and which results in the complete dissolution of the gel particles. Moreover, it was found that the ratio of the protein mass released during the fast phase relative to the slow phase could be controlled by varying the density of the gel network and the fraction of free to fibrillar protein; for gels that contained a large fraction of free protein, the fast phase involved the release of larger quantities of protein, suggesting that soluble protein molecules trapped in the pores of the microgel are released during this phase. In contrast, the slow phase can be attributed to the dissociation of molecules from the nanofibrils composing the gel. These results are consistent with other studies that show that the rate of dissolution of nanofibrils can take place over time scales of hours to days.[43]

We next investigated the potential of protein microgels to act as carriers for small molecules. The ability of lysozyme microgels to encapsulate drug-like molecules (Figure 3a and b), as well as their loading capacity, were studied for four types of compounds, including two dyes and two common drugs: ThT, Remazol Brilliant Blue R (RBBR), tetracycline and penicillin V. These molecules were selected to obtain a representative distribution in hydrophilicity and affinity to proteins. ThT is known for its strong affinity to amyloid structures, RBBR is an aromatic water-soluble reactive dye, tetracycline was chosen as representative of relatively hydrophobic water-soluble drug, and penicillin V is a water-soluble (hydrophilic) antibiotic. The small molecules were added to the precursor aqueous phase prior to capsule synthesis, and the final concentration of molecules encapsulated in the microgels was measured by UV absorption and fluorescence spectroscopy (see Methods). The data summarized in Figure 3c show that for all species an encapsulation efficiency in excess of 80% was achieved, confirming that the molecules were successfully incorporated into the gel particles.

We then focused on the release kinetics of the encapsulated species from the nanofibril microgels. To this effect, we incubated the microgels in deionized water for increasing periods of time, removed the gels by centrifugation, and measured the concentration of the small molecules released into the supernatant through their UV absorption (RBBR, ThT, tetracycline, penicillin V) or intrinsic fluorescence (ThT). The results shown in Figure 3d reveal marked differences in the rate of release of the small molecules. ThT exhibited the strongest affinity for the protein microgels and was not fully released even after 1 week, a result originating from the strong interaction of ThT with nanofibrils. By contrast, penicillin V reached its maximum release rate after 1 h and similar behavior was observed for RBBR and tetracycline.

We then examined the release kinetics in a cell culture medium designed to mimic physiological conditions. We found that under these conditions the lysozyme capsules had displayed a stability comparable to that observed in deionized water and that the release kinetics were not significantly affected by the biological medium α-MEM (see Supporting Information Figure S1c). The effect of pH on the kinetics of release was also probed over a broad pH range, from 1 to 12. The rate of the release of the four compounds from the capsules remained constant at low pH but was observed to change significantly at pH values above 9. At these higher pH values, the rate of degradation of the capsules was very rapid and was accompanied by the rapid release of the encapsulated cargomolecules (see Supporting Information Figure S3a and b).

The mechanism by which small molecules are released from the microgels was studied by following the morphological changes of the capsules by electron microscopy (Figure S4) as well as through the appearance of protein in the soluble phase (Figure S1c). The results reveal that the release mechanism of the encapsulated molecules from the lysozyme capsules follows a multistep process. In a first stage, unbound

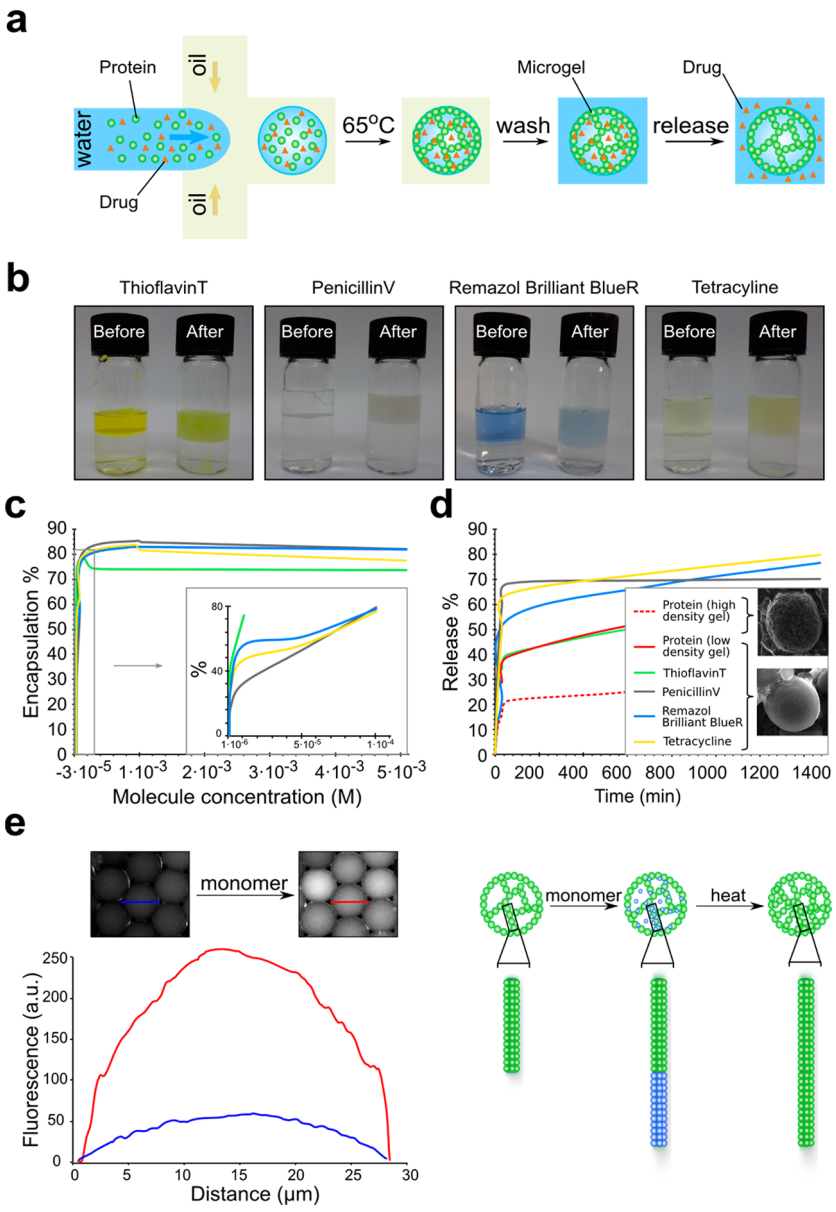

Figure 3. (a) Schematic representation of small molecule encapsulation and release from the lysozyme microgels. (b) Images of the precursor solutions containing a drug ("before") and the drug loaded microgels ("after") incorporation. (c) Encapsulation efficiency studies. The change in encapsulation efficiency was recorded as a function of small molecule concentration. (d) Release kinetics as a function of time. An inset images on the right panel show dense microgel particle (top) and a low dense particle (bottom). (e) Left panel: Fluorescence intensity profiles for the lysozyme gels before (blue) and after (red) incubation with protein monomer solution with images of the corresponding gels shown above the graph. Right panel: Schematic representation of lysozyme monomers incorporation into microgel fibrils.

small molecules in the vicinity of the interface are released into solution; a second slower time scale of release coincides with the dissolution of the capsules leading to the liberation of the remaining trapped molecules.

A particular feature of the microgels described in the present study, which exploits the dynamic nature of nanofibril assembly, is that they allow the density of the fibril network in their core is to be altered in response to exposure to monomeric precursor proteins even after the gel has been formed. As shown in Figure 3e, incubation of a lysozyme microgel within a solution that contains monomeric lysozyme results in the sequestration of additional monomers within the gel particle, leading to the growth of its component fibrils and an increase in the gel network density. Thus, unlike conventional gels based on synthetic polymers, the nanofibril microgels can undergo self-assembly processes to increase the density of the filament network in their core regimes even after they have formed, leading to a tunable dynamic material. This property may further allow the tailoring of chemical stability or reactivity of the nanofibril microgels.

Moreover, we explored whether or not the route discussed in this paper for the formation of protein

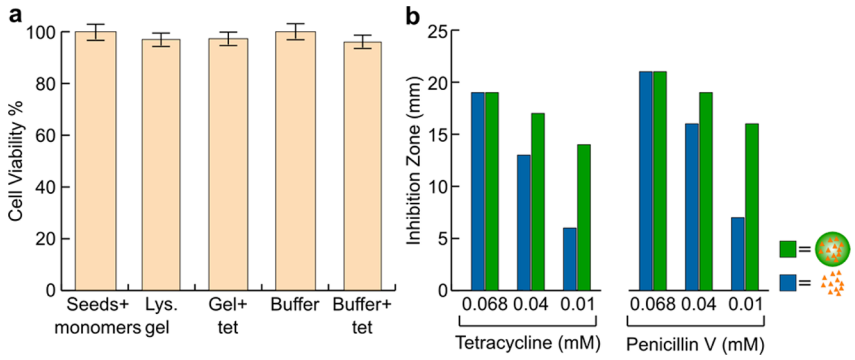

Figure 4. (a) Viability test with U2OS human cells. Cell viability was measured for the following solutions, left to right: precursor mixture of lysozyme seeds and lysozyme monomers, lysozyme microgel capsules, lysozyme capsules loaded with tetracycline drug, washing buffer from empty lysozyme capsules and washing buffer from tetracycline loaded lysozyme capsules. (b) Antibacterial activity of released tetracycline and penicillin V probed on S. areus. Inhibition zones obtained by exposure to the free drug in solution and to the drug encapsulated within lysozyme microgels were measured as a function of concentration. Blue columns represent the free drug and green columns the drug released from microgels.

microgels could be applied for structuring proteins or peptides that form fibrils under physiological conditions. We focused on a short hydrophilic peptide, called KD (see Methods), which has a propensity to form filaments under physiological pH and temperature. We carried out the microgel synthesis using this peptide as the building block, and the results presented in Figure S5 show that the microfluidic approach is suitable for structuring peptide nanofibrils that assemble under physiological conditions.

Finally, we investigated whether or not the increased local concentration of small molecule drugs, achieved through encapsulation, could lead to more effective pharmacological action. The antibacterial activities for the released tetracycline and penicillin V were probed using *Staphylococcus aureus* bacteria strains and were compared with the antibacterial activity exhibited by the antibiotics at the same concentrations in free solution in the absence of microgels (see Methods). For both antibiotics, the loaded microgels (Figure 4b) showed significantly enhanced antibacterial activity, by 20 and 60% for the low and high microgel concentrations, respectively. This enhanced antimicrobial activity can be rationalized by the higher local concentration of the antibiotic, which is achieved due to the spatial proximity of the antibiotic loaded microgels and the bacterial membrane, an interaction mediated by electrostatic attraction of the positively charged microgel particles and the negatively charged bacterial surface.

In order to establish the biocompatibility of the lysozyme capsules, toxicity assay were performed using human U2OS cells. To this effect, MTT assays[44] were performed to evaluate the viability of the cells after being exposed to the precursor mixture prior to gel formation, the lysozyme microgels, and the suspension containing released species from the lysozyme capsules. The results shown in Figure 4a demonstrate that none of the solutions were found to be toxic to the human cell line, which suggests that lysozyme microgels could be biocompatible as a drug delivery agent. We note that the use of preformed seed fibrils to initiate the protein aggregation leading to gelation allows the potentially toxic oligomeric stages[45,46] in protein aggregation to be avoided.

CONCLUSION

We have described an approach for generating microgels composed of amyloid fibril networks. These materials represent an artificial analog of naturally occurring three-dimensional amyloid-rich biofilms.[8] The protein nanofibril microgels are nontoxic to a human cell line and have the potential for effective drug encapsulation. In particular, we have demonstrated that the microgels enable the local release of encapsulated molecules resulting in enhanced antimicrobial action in the case of two common antibiotics, penicillin V and tetracycline. In addition, we have shown that the microgels are dynamic materials that enable the internal content of nanofibrils to be changed at the postsynthetic stage in response to exposure to monomeric protein molecules in solution. Thus, protein nanofibril microgels represent a class of biomaterials that exhibit a number of advantageous features as a result of their noncovalent assembly from natural building blocks.

METHODS

Droplet Microfluidics. The microfluidic droplet maker was fabricated in polydimethylsiloxane (PDMS) using soft lithography techniques.[47,48] Microdroplets were generated by flow-focusing[43] from an aqueous solution of 6% (w/w) lysozyme (from hen egg white, Sigma–Aldrich) in 120 mM HCl and 19.5 mM NaCl and 1.9 ppm (w/v) NaN_3 and a continuous outer phase consisting of FC40 (Sigma–Aldrich) fluorinated oil

containing 2% w/v of *N*,*N*′-bis(*n*-propyl)poly(ethylene oxide)-bis(2-trifluoromethyl polyperfluoroethylene oxide) amide surfactant. The surfactant was synthesized as previously described.[49] The aqueous phase contained 2% w/w preformed seed aggregates to accelerate the conversion of protein monomers into fibrillar form (except for the studies shown in Figure 2 where the concentration was varied as indicated in the caption). The lysozyme seed aggregates were formed by incubating (with magnetic stirring) an initially monomeric lysozyme solution 3.4 mM for 48 h at 65 °C in acid 120 mM HCl prepared in doubly distilled water (DDW). After the lysozyme monomers were converted into nanofibrils, the aggregates were exposed to probe sonication for 1 min in order to promote fibril breakage into small fragments.

The Ac-KGSFSIQYTYHVD-$CONH_2$ peptide (here called KD peptide) is derived from human semenogelin I protein as a two-residue extended version of a peptide which was recently found to form a pH-tunable hydrogel.[50] Microdroplets of the KD peptide were generated by flow-focusing from an aqueous solution of 0.4 mg/mL KD peptide in doubly distilled water (immediately after dissolution of lyophilized peptide powder) and a continuous outer phase consisting of FC40 (Sigma–Aldrich) fluorinated oil containing 2% w/v of *N*,*N*′-bis(*n*-propyl)-poly(ethylene oxide)-bis(2-trifluoromethyl polyperfluoroethylene oxide) amide surfactant.

Microgel Formation. After the microdroplets were formed, they were incubated for 24 h at 65 °C in order to promote gelation. To separate the microgels from the continuous oil phase and from the protein molecules which did not incorporate into the fibril microgels, 500 μL of 10 mM HCl was added to a 1 mL of microgel suspension in FC40, mixed, and then centrifuged at 700 rpm for 1 min. The emulsion phase at the oil–water interface was collected and this washing procedure repeated 3 times. For encapsulation studies the precursor drug molecules were mixed with aqueous solutions of lysozyme. The conditions used were as follows: (1) ThT was dissolved in doubly distilled acidified water (pH = 2), at a concentration of 6.58×10^{-5} M; (2) RBBR in acidified water (pH = 4) at a concentration of 7.31×10^{-5} M; (3) penicillin V 9.4×10^{-4} M in acidified water (pH = 2); and (4) tetracycline in water (pH = 5) at a concentration of 9.10×10^{-4} M. The formation of microgels at different pH was studied for pH values 2.4 and 5.5. For gelation of KD peptide droplets, the collected solution was incubated at 4°C overnight.

Measurements of Efficiency, Encapsulation Capacity, and Release Kinetics. The loaded microgels were washed with 10 mM HCl at intervals of time ranging from 10 min to 14 days with DDW and α-MEM media at 37 °C. The solutes after each washing were analyzed by UVspectroscopy. Release media for acidic pH was prepared by adding HCl to DDW and for basic by adding NaOH to DDW. The encapsulation efficiencies we calculated by subtracting the concentration of drug-like molecules in residue solution from the total concentration of drug in precursor mixture. The measurements were repeated for different drug concentrations. The concentrations of released components were calculated by subtracting the concentration measured in the washing solution from the total concentration of encapsulated drug-like molecules.

Confocal Microscopy. For confocal fluorescent microscopy, samples were prepared by depositing the aqueous dispersions, without further purification, onto glass slides. The protein microgels were analyzed using a confocal microscope (Laser Scan Confocal, Zeiss Microscope) with the following lasers: UV405 nm at 25 mW (for violet excitation) and Argon 458/477/488/514 nm at 30 mW (for green excitation). The 3D images were reconstructed using the Imaris image analysis software (on average 235 z-stack slices per each protein shell).

Scanning Electron Microscopy. In order to keep the spherical shape of the protein gels intact, the microgels were deposited onto rounded coverslip glass slides and dried under low vacuum conditions in a chamber with a pressure of 1×10^{-3} mbar, pumping rate 1×10^{-5} mbar·L/s, 25 °C. After drying, a 20 nm gold layer was deposited using a vacuum sputtering coater (Denton Vacuum Desk IV). and the sample was imaged with a JEOL JSM-840 SEM. Cryo-SEM images were obtained using FEI version 460 microscope (equipped with Quorum cryo-transfer system) after 20 nm gold coating deposition, at 5 kV.

Atomic Force Microscopy. For atomic force microscopy (AFM) lysozyme monomers, seeds, fibrils and microgels were deposited on mica slides and dried at ambient conditions. The lysozyme nanofibril microgels were washed with DDW and centrifuged for 15 min at 13 000 rpm. This washing procedure was repeated 5 times. The samples were then analyzed and characterized by AFM microscope, H-02-0067 Nano Wizard II, tapping mode (JPK Instruments).

FTIR Structural Analysis. The structural analysis of the lysozyme microgel and lysozyme fibrils was performed by using an FTIR-Equinox 55 spectrometer (Bruker). The samples (washed with DDW), without further pretreatment, were loaded to the FTIR sample holder and analyzed by subtracting a water reference. The carbon dioxide atmospheric compensation was subtracted from the original FTIR spectra, and a secondary derivative was applied for further analysis.

Capsule Dissociation. The morphological changes (using SEM and TEM) of the capsules were followed as a function of washing time in DDW. We observed that protein molecules first detached from the outer surface of the capsule (Figure S4). Then, pores were detected on the surface of the capsules, which grew in size as a function of size up to 300 nm size after 12 h. The morphology of the released species also changed with increases in washing times. During the first 12 h the released species had spherical nanoparticulate form, but after 12 h larger aggregated species were observed to be released. These results indicate that initially the outer surface of the capsule loses a protein layer and then pores are created that the lysozyme fibrils that form the inner sphere of the capsules to dissociate. Finally, dissociation of the entire capsule was observed.

CD Analysis. The degree of aggregation of the lysozyme protein in bulk solution and in microdroplets was measured by CD analysis, following the change in β-sheet content. The structural analysis of the microcapsules was performed by using CD-J810 (JASCO) spectropolarimeter. The samples were loaded to the CD cuvette and analyzed. The following samples were analyzed by CD spectroscopy: monomeric lysozyme, fibrillar lysozyme and protein extracted from microgels by ultrafast centrifugation (13 000 rpm, 30 min).

ThT Assay. The incorporation of lysozyme monomers into the fibrillar structures within the microgels was studied by following the changes in the fluorescent emission intensity of ThT dye at 490 nm. ThT dye at by the 7×10^{-5} M concentration was added to the droplets formed by microfluidic method and incubated for 24 h at 4 °C.

After gelation was accomplished, the microcapsules were washed with DDW to remove the surfactant, unreacted molecules and an excess of ThT dye. The fluorescent intensity of the gels was monitored by fluorescent plate reader Fluorostar (BMG Labtech) using a ThT filter (excitation 440 nm/emission 490 nm).

Antibacterial Assays. The activity of the two types of antibiotics tetracycline and penicillin V was probed and inhibition zones were compared with three sets of diluted solutions of the free antibiotics. The drops of solution were positioned on agar plates containing bacterial strains (O.D. 0.3), and inhibition zones were measured after 28 h.

Toxicity Assays. 2 mL U20S cells (1.8×10^{-4}) were incubated in low glucose DMEM media34 with 0.5 mL of following solutions for 48 h at 37 °C: (1) the precursor solution of lysozyme monomers and lysozyme seeds; (2) lysozyme microgels; (3) washing solution from lysozyme gels; (4) lysozyme gels loaded with tetracycline; (5) washing solution of the tetracycline loaded lysozyme microgels. The incubation medium was first removed (centrifugation at 300*g* for 5 min at 4 °C), then cells were transferred into smaller volume plates and the media was exchanged with 80 μL of fresh solution. A 20 μL portion of MTT (3-[4,5-dimethylthiazol-2-yl]-2,5-diphenyltetrazolium bromide, Sigma) was then added (5 mg/mL stock solution) and the cells were incubated at 37 °C for 3 h. The medium was removed, and then150 μL of DMSO was added and the system allowed to incubate for 10 min. The solutions were then mixed by pipetting, and the absorbance of each well at 570 nm was measured. Because of the physical state of gelled particles, the toxicity measurements were performed on particle fragments obtained

after extended centrifugation were performed only on liquid disassembled particles.

Conflict of Interest: The authors declare no competing financial interest.

Acknowledgment. We thank Elan Pharmaceuticals (US, TOM, CMD, TPJK), BBSRC (TPJK), the Leverhulme Trust (AKB), ERC (TPJK), Frances and Augustus Newman Foundation (TOM, TPJK) and Magdalene College, Cambridge (AKB) for financial support and Prof. S. Michaeli for helpful advice regarding toxicity measurements. Part of the work described here has been the subject of a patent application filed by Cambridge Enterprise, Ltd.

Supporting Information Available: Figures S1–S5. This material is available free of charge *via* the Internet at http://pubs.acs.org.

REFERENCES AND NOTES

1. Knowles, T. P. J.; Buehler, M. J. Nanomechanics of Functional and Pathological Amyloid Materials. *Nat. Nanotechnol.* **2011**, *6*, 469–479.
2. Paparcone, R.; Keten, S.; Buehler, M. J. Atomistic Simulation of Nanomechanical Properties of Alzheimer's Abeta(1–40) Amyloid Fibrils under Compressive and Tensile Loading. *J. Biomech.* **2010**, *43*, 1196–1201.
3. Adamcik, J.; Lara, C.; Usov, I.; Jeong, J. S.; Ruggeri, F. S.; Dietler, G.; Lashuel, H. A.; Hamley, I. W.; Mezzenga, R. Measurement of Intrinsic Properties of Amyloid Fibrils by the Peak Force QNM Method. *Nanoscale* **2012**, *7*, 4426–4429.
4. Fowler, D. M.; Koulov, A. V.; Alory-Jost, C.; Marks, M. S.; Balch, W. E.; Kelly, J. W. Functional Amyloid Formation within Mammalian Tissue. *PLoS Biol.* **2006**, *4*, e6.
5. Li, C.; Bolisetty, S.; Mezzenga, R. Hybrid Nanocomposites of Gold Single-crystal Platelets and Amyloid Fibrils with Tunable Fluorescence, Conductivity, and Sensing Properties. *Adv. Mater.* **2013**, *25*, 3694–3700.
6. Liu, T.; Seiffert, S.; Thiele, J.; Abate, A. R.; Weitz, D. A.; Richtering, W. Non-coalescence of Oppositely Charged Droplets in pH-sensitive Emulsions. *Proc. Natl. Acad. Sci. U. S. A.* **2012**, *109*, 384–389.
7. Adler-Abramovich, L.; Aronov, D.; Gazit, E.; Rosenman, G. Patterned Arrays of Ordered Peptide Nanostructures. *J. Nanosci. Nanotechnol.* **2009**, *9*, 1701–1708.
8. Kelly, J. W. Towards an Understanding of Amyloidogenesis. *Nat. Struct. Biol.* **2002**, *9*, 323–325.
9. Cao, A.; Hu, D.; Lai, L. Formation of Amyloid Fibrils from Fully Reduced Hen Egg White Lysozyme. *Protein Sci.* **2004**, *13*, 319–324.
10. Greenwald, J.; Riek, R. Biology of Amyloid: Structure, Function, and Regulation. *Structure* **2010**, *18*, 1244–1260.
11. Yan, H.; Frielinghaus, H.; Nykanen, A.; Ruokolainen, J.; Saiani, A.; Miller, A. F. Thermoreversible Lysozyme Hydrogels: Properties and an Insight into the Gelation Pathway. *Soft Matter* **2008**, *4*, 1313–1325.
12. Jiang, L.; Liu, C.; Leibly, D.; Landau, M.; Zhao, M.; Hughes, M. P.; Eisenberg, D. S. Structure-based Discovery of Fiber-binding Compounds that Reduce the Cytotoxicity of Amyloid Beta. *eLife* **2013**, *2*, e00857.
13. Leitner, A.; Joachimiak, L. A.; Bracher, A.; Monkemeyer, L.; Walzthoeni, T.; Chen, B.; Pechmann, S.; Holmes, S.; Cong, Y.; Ma, B.; *et al.* The Molecular Architecture of the Eukaryotic ChaperoninTRiC/CCT. *Structure* **2012**, *20*, 814–825.
14. Bolisetty, S.; Vallooran, J. J.; Adamcik, J.; Handschin, S.; Gramm, F.; Mezzenga, R. Amyloid-Mediated Synthesis of Giant, Fluorescent, Gold Single Crystals and Their Hybrid Sandwiched Composites Driven by Liquid Crystalline Interactions. *J. Colloid Interface Sci.* **2011**, *361*, 90–96.
15. Phan-Xuan, T.; Durand, D.; Nicolai, T.; Donato, L.; Schmitt, C.; Bovetto, L. On the Crucial Importance of the pH for the Formation and Self-Stabilization of Protein Microgels and Strands. *Langmuir* **2011**, *27*, 15092–15101.
16. Sagis, L. M. C.; de Ruiter, R.; Miranda, F. J. R.; de Ruiter, J.; Schroën, K.; van Aelst, A. C.; Kieft, H.; Boom, R.; van der Linden, E. Polymer Microcapsules with a Fiber-Reinforced Nanocomposite Shell. *Langmuir* **2008**, *24*, 1608–1612.
17. Humblet-Hua, N.-P. K.; van der Linden, E.; Sagis, L. M. C. Microcapsules with Protein Fibril Reinforced Shells: Effect of Fibril Properties on Mechanical Strength of the Shell. *J. Agric. Food Chem.* **2012**, *60*, 9502–9511.
18. Knowles, T. P. J.; Oppenheim, T. W.; Buell, A. K.; Chirgadze, D. Y.; Welland, M. E. Nanostructured Films from Hierarchial Self-assembly of Amylogenic Proteins. *Nat. Nanotech.* **2010**, *5*, 204–207.
19. Zhang, S. Fabrication of Novel Biomaterials Through Molecular Self-assembly. *Nat. Biotechnol.* **2003**, *21*, 1171–1178.
20. Maji, S. K.; Schubert, D.; Rivier, C.; Lee, S.; Rivier, J. E.; Riek, R. Amyloid as a Depot for the Formulation of Long-Acting Drugs. *PLoS Biol.* **2008**, *6*, e17.
21. Humblet-Hua, K.; Scheltens, G.; van der Linden, E.; Sagis, L. Encapsulation Systems Based on Ovalbumin Fibrils and High Methoxyl Pectin. *Food Hydrocolloids* **2011**, *25*, 569–576.
22. Bai, S.; Debnath, S.; Gibson, K.; Schlicht, B.; Bayne, L.; Zagnoni, M.; Ulijn, R. V. Biocatalytic Self-Assembly of Nanostructured Peptide Microparticles Using Droplet Microfluidics. *Small* **2014**, *10*, 285–293.
23. Bai, S.; Pappas, C.; Debnath, S.; Frederix, PW. J. M.; Leckie, J.; Fleming, S.; Ulijn, R. V. Stable Emulsions Formed by Self-assembly of Interfacial Networks of Dipeptide Derivatives. *ACS Nano* **2014**, *8*, 7005–7013.
24. Rozkiewicz, D. I.; Myers, B. D.; Stupp, S. I. Interfacial Self-assembly of Cell-like Filamentous Microcapsules. *Angew. Chem., Int. Ed.* **2011**, *50*, 6324–6327.
25. Shimanovich, U.; Knowles, T. P. J.; Weitz, D. A.; Dobson, C. M.; Cambridge Enterprise, Ltd. Protein Capsules. Patent application. GB 1415681.4. 2014.
26. Shimanovich, U.; Knowles, T. P. J.; Holland, C. Silk Protein Structures. Patent application. GB 1415679.8. 2014.
27. Seiffert, S.; Thiele, J.; Abate, A. R.; Weitz, D. A. Smart Microgel Capsules from Macromolecular Precursors. *J. Am. Chem. Soc.* **2010**, *132*, 6606–6609.
28. Jia, X.; Yeo, Y.; Clifton, R. J.; Jiao, T.; Kohane, D. S.; Kobler, J. B.; Zeitels, S. M.; Langer, R. Hyaluronic Acid-based Microgels and Microgel Networks for Vocal Fold Regeneration. *Biomacromolecules* **2006**, *7*, 3336–3344.
29. Li, C.; Adamcik, J.; Mezzenga, R. Biodegradable Nanocomposites of Amyloid Fibrils and Graphene with Shape-Memory and Enzyme-Sensing Properties. *Nat. Nanotechnol.* **2012**, *7*, 421–427.
30. Suh, S. K.; Yuet, K.; Hwang, D. K.; Bong, K. W.; Doyle, P. S.; Hatton, T. A. Synthesis of Nonspherical Superparamagnetic Particles: *In Situ* Coprecipitation of Magnetic Nanoparticles in Microgels Prepared by Stop-Flow Lithography. *J. Am. Chem. Soc.* **2012**, *134*, 7337–7343.
31. Bartus, R. T.; Tracy, M. A.; Emerich, D. F.; Zale, S. E. Sustained Delivery of Proteins for Novel Therapeutic Agents. *Science* **1998**, *281*, 1161–1162.
32. Peer, D.; Karp, J. M.; Hong, S.; Farokhzad, O. C.; Margalit, R.; Langer, R. Nanocarriers as an Emerging Platform for Cancer Therapy. *Nat. Nanotechnol.* **2007**, *2*, 751–760.
33. Knowles, T. P. J.; Vendruscolo, M.; Dobson, C. M. The Amyloid State and its Association with Protein Misfolding Diseases. *Nat. Rev. Mol. Cell Biol.* **2014**, *15*, 384–396.
34. Langer, R.; Tirrell, D. A. Designing Materials for Biology and Medicine. *Nature* **2004**, *428*, 487–492.
35. Booth, D. R.; Sunde, M.; Bellotti, V.; Robinson, C. V.; Hutchinson, W. L.; Fraser, P. E.; Hawkins, P. N.; Dobson, C. M.; Radford, S. E.; Blake, C. C.; *et al.* Instability, Unfolding and Aggregation of Human Lysozyme Variants Underlying Amyloid Fibrillogenesis. *Nature* **1997**, *385*, 787.
36. Dobson, C. M. A Camelid Antibody Fragment Inhibits the Formation of Amyloid Fibrils by Human Lysozyme. *Nature* **2003**, *426*, 884–890.
37. Feng, G.-D.; Zhang, F.; Cheng, L.-H.; Xu, X.-H.; Zhang, L.; Chen, H.-L. Evaluation of FT-IR and Nile Red Methods for Microalgal Lipid Characterization and Biomass Composition Determination. *Bioresour. Technol.* **2013**, *128*, 107–112.

38. Hunter, R. J. *Zeta Potential in Colloid Science: Principles and Applications*; Academic Press: Waltham, MA, **1981**.
39. Shimanovich, U.; Tkacz, I. D.; Eliaz, D.; Cavaco-Paulo, A.; Michaeli, S.; Gedanken, A. Encapsulation of RNA Molecules in BSA Microspheres and Internalization into *Trypanosoma brucei* Parasites and Human U2OS Cancer Cells. *Adv. Funct. Mater.* **2011**, *21*, 3659–3666.
40. Jarrett, J. T.; Lansbury, P. T. Seeding "One-dimensional Crystallization" of Amyloid: a Pathogenic Mechanism in Alzheimer's Disease and Scrapie? *Cell* **1993**, *73*, 1055–1058.
41. Lorenzen, N.; Cohen, S. I. A.; Nielsen, S. B.; Herling, T. W.; Christiansen, G.; Dobson, C. M.; Knowles, T. P. J.; Otzen, D. Role of Elongation and Secondary Pathways in S6 Amyloid Fibril Growth. *Biophys. J.* **2012**, *102*, 2167–2175.
42. Hsu, J. C.-C.; Chen, E. H.-L.; Snoeberger, R. C. r.; Luh, F. Y.; Lim, T.-S.; Hsu, C.-P.; Chen, R.P.-Y. Thioflavin T and Its Photoirradiative Derivatives: Exploring Their Spectroscopic Properties in the Absence and Presence of Amyloid Fibrils. *J. Phys. Chem. B* **2013**, *4*, 3459–3468.
43. Carulla, N.; Caddy, G. L.; Hall, D. R.; Zurdo, J.; Gairí, M.; Feliz, M.; Giralt, E.; Robinson, C. V.; Dobson, C. M. Molecular Recycling Within Amyloid Fibrils. *Nature* **2005**, *436*, 554–558.
44. Cole, S. P. Rapid Chemosensitivity Testing of Human Lung Tumor Cells Using the MTT Assay. *Cancer Chemother. Pharmacol.* **1986**, *17*, 259–263.
45. Bucciantini, M.; Giannoni, E.; Chiti, F.; Baroni, F.; Formigli, L.; Zurdo, J.; Taddei, N.; Ramponi, G.; Dobson, C. M.; Stefani, M. Inherent Toxicity of Aggregates Implies a Common Mechanism for Protein Misfolding Diseases. *Nature* **2002**, *416*, 507–11.
46. Kayed, R.; Head, E.; Thompson, J. L.; McIntire, T. M.; Milton, S. C.; Cotman, C. W.; Glabe, C. G. Common Structure of Soluble Amyloid Oligomers Implies Common Mechanism of Pathogenesis. *Science* **2003**, *300*, 486–489.
47. Qin, D.; Xia, Y.; Whitesides, G. Soft Lithography for Micro- and Nanoscale Patterning. *Nat. Protoc.* **2010**, *5*, 491–502.
48. Anna, S.; Bontoux, N.; Stone, H. Formation of Dispersions Using "Flow Focusing" in Microchannels. *Appl. Phys. Lett.* **2003**, *82*, 364–366.
49. Holtze, C.; Rowat, A.; Agresti, J.; Hutchison, J.; Angilè, F.; Schmitz, C.; Köster, S.; Duan, H.; Humphry, K.; Scanga, R.; *et al.* Biocompatible Surfactants for Water-in-fluorocarbon Emulsions. *Lab Chip* **2008**, *8*, 1632–1639.
50. Frohm, B.; DeNizio, J. E.; Lee, D. S. M.; Gentile, L.; Olsson, U.; Malm, J.; Åkerfeldt, K. S.; Linse, S. A Peptide from Human Semenogelin I Self-Assembles into a pH-Responsive Hydrogel. *RSC Soft Matter* **2014**, 10.1039/C4SM01793E.